Atmos. Meas. Tech. Discuss., https://doi.org/10.5194/amt-2017-405
Manuscript under review for journal Atmos. Meas. Tech.
Discussion started: 20 December 2017

Atmospheric Measurement Techniques
Discussions

# Inter-channel uniformity of a microwave sounder in space

Martin Burgdorf[1], Imke Hans[1], Marc Prange[1], Theresa Lang[1], and Stefan A. Buehler[1]

[1]Universität Hamburg, Faculty of Mathematics, Informatics and Natural Sciences, Department of Earth Sciences, Meteorological Institute, Bundesstraße 55, 20146 Hamburg, Germany

*Correspondence to:* Martin Burgdorf (martin.burgdorf@uni-hamburg.de)

**Abstract.**

We analyzed intrusions of the Moon in the deep space view of the Advanced Microwave Sounding Unit-B on the NOAA-16 satellite and found no significant discrepancies in the signals from the different sounding channels between 2001 and 2008. Earlier investigations, however, had detected biases of up to 10 K by using simultaneous nadir overpasses of NOAA-16 with other satellites. These discrepancies in the observations of Earth scenes cannot be due to non-linearity of the receiver or contamination of the deep space view without affecting the signal from the Moon as well. As major anomalies of the on-board calibration target and frequency shifts of the local oscillator were not present, either, the most obvious reason for the degrading photometric stability is radio frequency interference in combination with a strongly decreasing gain. By means of the chosen example we demonstrate the usefulness of the Moon for investigations of the performance of microwave sounders in flight.

## 1 Introduction

Photometric stability of the measurement devices is an indispensable prerequisite for a reliable characterization of global change in atmospheric properties. This basic rule is particularly valid for space-based instruments, because they cannot be checked in the laboratory again once the operational phase has begun. Microwave sounders take therefore advantage of an on-board calibration target (OBCT) for updating the flux calibration in intervals of a few seconds. Nevertheless systematic errors can creep in from slowly changing instrumental properties that cannot be detected with the generally employed two-point calibration, for example non-linearity. In order to first characterize and then reduce these errors in the case of AMSU-A (Advanced Microwave Sounding Unit-A), Zou and Wang (2011) determined time-dependent calibration offsets and nonlinear coefficients from simultaneous nadir overpass (SNO) regressions, which resulted in more consistent multi-satellite radiance observations for all respective channels. SNOs and other inter-calibration methods, however, that rely exclusively on the comparison of two space instruments without a third source of information about the Earth scenes, can, as a matter of principle, never remove all spurious trends in the data, because they cannot identify the relative contributions of either instrument to offsets and drifts.

At first sight it seems impossible to transfer the method developed by Zou and Wang (2011) to the sounding channels of AMSU-B (channels 18-20), because their departure from linearity was proven to be smaller than 0.1 K and basically independent of instrument temperature in ground tests (Saunders et al. , 1995b). As a consequence the nonlinear coefficient for the sounding channels was supposed to be insignificant and set to zero in the calibration files used by AAPP (ATOVS [Advanced TIROS-N {Television and InfraRed Observation Satellite} Operational Vertical Sounder] and AVHRR [Advanced Very High Resolution Radiometer] Pre-processing Package) for AMSU-B on all platforms. Nevertheless there were considerable biases between the sounding channels of AMSU-B on NOAA-16 and those on other satellites, especially towards the end of its lifetime (John et al. , 2012; Hanlon and Ingram , 2015) and particularly pronounced with channel 20. In this work we investigate why the flux calibration of the different channels seemed to diverge with time by using the radiation from the Moon when entering the deep space view (DSV) as a third reference flux, in addition to the Cosmic Microwave Background (CMB) and the OBCT. We concentrate on the three sounding channels, because they are the scientifically most important ones, characterizing the 183.3 GHz line of water vapor, and at the same time apparently the worst with respect to stability.

As the Moon fills only a fraction of the beam, it is particularly well suited to detect effects, whose impact grows with decreasing scene flux. On top of that its microwave spectrum differs considerably from Earth's, for it is featureless and varies little with wavelength (Mangum , 1993). This means that all channels with the same central frequency, i. e. the three sounding channels, must produce the same brightness temperature when observing the Moon[1]. With this approach it seemed therefore feasible to throw additional light on the origin of the biases of AMSU-B on NOAA-16, which have defied explanation until now.

## 2 Observations and methods

### 2.1 Selection of Moon intrusions

As the different sounding channels of AMSU-B observe at the same time with the same center frequency and in the same direction, there is no need to know the brightness temperature of the Moon for studies of the inter-channel uniformity, for every channel gets the same flux. It is advantageous, however, to select those intrusions, where the Moon comes closest to the center of the beam. This is not only because one gets the strongest signal with this alignment, but also because the "light curve",

---

[1] Apart from a very small band correction

i. e. the measured brightness temperature as a function of time, resembles most closely a Gaussian in this case, making it easy to determine its maximum value without introducing systematic errors from the fit. The minimum distance between the pointing direction of each DSV and the Moon can be calculated for each orbit with AAPP, providing the information needed to identify candidates for further investigation. We concentrated our search on the years 2001, 2004, 2006, and 2007, thus increasing the density of observations at the start of the mission and the period of the emerging bias pattern. Beginning with the year 2007, the decreasing signal-to-noise ratio started to affect the accuracy of the photometric measurements (Hans et al. , 2017).

### 2.2 Analysis

We fit the light curves of the Moon, which are sampled once per scan, with a Gaussian. The fit is achieved by optimizing three parameters: the maximum number of counts $a$, the centroid (location) $\mu$, and the peak width $\sigma$. Each of these parameters provides information about a different property of the instrument: gain, pointing direction in the along-track direction, and beam size in the along-track direction. If the Moon appears in three DSVs at the same time, it is possible to fit a Gaussian through the maximum signal of each of them and thus to obtain information about the beam pattern in the across-track direction as well, see Fig. 1. Obviously the Moon produces a signal in all frequency channels, but the signal-to-noise ratio varies considerably among the different channels.

For an investigation of photometric stability and uniformity the value of $a$ and the minimum distance of the Moon to the pointing direction of the DSVs need to be known. This is because $a$ is a function of this distance and the beam pattern.

#### 2.2.1 Position of the beam

AAPP calculates the lunar angles for each scan and all four DSVs and writes part of this information in the level 1b file. It is therefore possible to identify the smallest lunar angle for each DSV. Unfortunately the calculation with AAPP is subject of several uncertainties:

- The error in the moon calculation is at worst 0.3° (EUM.EPS.SYS.SPE.990006 , 2013). This value has been confirmed by the analysis of Moon intrusions in Burgdorf et al. (2016). It is caused by incomplete knowledge of the alignment of the satellite; the position of the Moon is known with very high accuracy.
- Misalignment of the quasi-optics or feedhorns would be likely to produce effects on Channels 18, 19, and 20 which share the path to the receiver (McLellan , 1998). Such a misalignment could have been caused by vibrations during launch and is difficult to detect during flight, since Ground Control Points cannot be used with the sounding channels. So for the utilization

period of AMSU-B on NOAA-16, no geolocation correction is performed on data from MW instruments aboard the NOAA satellites (Moradi et al. , 2011).

- The position of the warmest spot on the lunar surface varies with phase and is therefore in general not in the center. Given the fact that the Moon can only appear with phases $\pm$ 60° around full Moon in the DSV (Burgdorf et al. , 2016), its temperature maximum cannot be off centre by more than half of the Moon's apparent radius, i. e. $\approx 0.1°$ (Coates , 1961).

For these reasons one cannot rely on the calculation with AAPP to determine the lunar angles of the different Moon intrusions. Instead the point of maximum signal was first identified in the along-track direction from the light curve in each DSV (Fig. 1). Then we determined the point of maximum signal in the across-track direction, i. e. in the scan plane, by fitting a Gaussian to the maximum signal $a_i$ from each DSV, $1 \leq i \leq 4$. This procedure requires a detection of the Moon with a good signal-to-noise ratio in three DSVs, as shown in Fig. 1, since the fitting procedure uses three independent parameters. The value for $\mu$ obtained this way was multiplied by the difference in $\theta$ between two neighbouring DSVs, which is $1.1°$ with AMSU-B and MHS, and then compared to the value calculated with AAPP in Table 1. These new lunar angles formed the basis for the final selection of intrusion events from the provisional shortlist based on the lunar angles calculated with AAPP (see Sect. 2.1).

### 2.2.2 Brightness temperatures

The value for $a$ from the second Gauss fit gives now the number of counts the Moon would have provided, if it had been in the center of the DSV, and it was used, after division by the gain, to calculate the ratios of the brightness temperatures in channels 18/19 and 20 (last column in Table 1). The values from channels 18 and 19 were averaged in order to reduce the noise in the reference, to which channel 20, the one with the highest bias (see Sect. 1), is compared. In cases where the Moon could only be detected in two DSVs, we used the brightness temperatures as measured in the DSV that came closest to the Moon. This method was only applied, when we could conclude from the relative strengths of the signals in the two DSVs, where the Moon appeared, that the lunar angle must have been very small ($< 0.2°$) in one of them. This way the impact of pointing uncertainties on the signal from the Moon is kept as small as possible. Our values, however, do not represent the actual temperature of the Moon, because we did not correct for the fact that it does not fill the beam.

### 2.2.3 Beam pattern

An important characteristic of the beam, namely its full width at half maximum, follows immediately from the peak width of the Gauss fit, which is related to the full width half maximum via $\sigma = FWHM \,/\, \sqrt{8 \cdot ln2}$. In the across-track direction, where the Moon can only be detected in three DSVs with sufficient signal-to-noise ratio, it is less accurate than in the along-track direction, where the FWHM of the beam can be determined from light curves with dozens of points. Random samples showed no significant deviations from the nominal value of $1.1°$ for the FWHM of the beam.

### 2.3 Inter-band calibration (18 - 20)

As the brightness temperature of the disk-integrated Moon as seen by the microwave sounders is always more than 200 K (Eq. (5) in Yang and Weng , 2016), the Rayleigh-Jeans approximation of Planck's law is applicable[2], and its spectral radiance is proportional to the product of temperature and frequency squared. This means that the maximum signal from a Moon intrusion in counts, divided by the gain, should be the same for all sounding channels. Differences can be caused, however, by the following effects:

- Imperfect co-registration of the channels: The Moon comes closer to the pointing direction of one channel than the pointing direction of another. This is unlikely, however, because all sounding channels share the path to the receiver (see Sect. 2.2.1). The difference in signal between a lunar angle of $0.05°$ and one of $0.15°$ - more than what was found for uncorrelated channels by Bonsignori (2017) - is only 1%, assuming a Gaussian light curve and a FWHM of the beam of $1.1°$. We consider therefore this effect negligible.
- Incorrect gain values: The uncertainty associated with the gain has been calculated for the time of each Moon intrusion and is included in Table 1. The gain value assigned to the time of the Moon intrusion was obtained from interpolating the mean values a short time before and after the intrusion. The uncertainty of this gain value was then estimated from the variation of the gain values before and after the intrusion. We note that any error in the value for radiance/temperature of DSV and OBCT that was used in calculating the gain cancels out in the following calculations, because we consider only ratios between the channels.
- Incorrect frequency values, due to an irregular relative spectral response function or a drift of the local oscillator. According to the Rayleigh-Jeans Law the ratio between the maximum signals from light curves measured at two similar frequencies is twice the ratio of these frequencies. This means that a shift of 1 GHz in one of the sounding channels changes the signal by about 1%.
- The brightness temperature $T_b$ of the Moon varies slowly with frequency, and so does the phase angle, for which it reaches its maximum value (Keihm , 1983, http://lunar-model-brightness-temperatures.net). In very good approximation, however, $T_b$ is the same for all sounding channels, because they have the same central frequency: 183.3 GHz.

---

[2] The difference between the spectral radiances at 200 K and 183 GHz according to Planck and Rayleigh-Jeans amounts to 2%.

A common misalignment of all channels is irrelevant for our analysis, because it affects them all in the same way, and any reasonable error in frequency should be negligible: Its temperature coefficient is typically 1 MHz/K (Saunders , 1994). Hence it is possible to verify the stability of the gain ratio between different sounding channels, i. e. their inter-band calibration, with an accuracy that is essentially limited by the uncertainties of the gain and the parameters of the Gaussian fit.

## 2.4 Results

### 2.4.1 Uniformity of flux calibration

The average ratio between the signals obtained in channels 18/19 and 20 is $1.001 \pm 0.006$ for all observations in Table 1 combined. It is $0.993 \pm 0.008$ for the twelve values from the years 2001 and 2004 and $1.007 \pm 0.008$ for the later Moon intrusions. Within the error margins these figures are in agreement with the values derived by John et al. (2012) and Hanlon and Ingram (2015) from simultaneous nadir overpasses.

### 2.4.2 Across-track pointing accuracy

For a comparison of the pointing directions of DSVs two and three in the across-track direction as calculated with AAPP (min moon angle) and with the aid of a Gauss fit (see Sect. 2.2.1), we consider now only the years 2001 and 2004, because the noise was lowest in the beginning of the mission. We find a difference of $-0.113° \pm 0.019°$, i. e. the DSV direction determined with the Gauss fit leads the one calculated with AAPP by about $0.1°$. The systematic error in the absolute pointing direction of the sounding channels of AMSU-B on NOAA-16 lies well below the upper limit of the overall, i.e. across- and along-track, pointing error of $0.2°$ for channel 16 that was given by Atkinson (2000b).

## 2.5 Discussion

In the following we identify the reason for the trends found by John et al. (2012) and others in the sounding channels of AMSU-B on NOAA-16 with the aid of the results obtained from our analysis of the Moon intrusions. We start with the measurement equation for microwave sounders Eq. (1), as it is usually found in the literature, (e. g. Labrot et al. , 2011; EUM.EPS.SYS.SPE.990006 , 2013; Weng and Yang , 2016).

$$R_\mathrm{s} = R_\mathrm{w} + (C_\mathrm{s} - \overline{C}_\mathrm{w}) \cdot \frac{R_\mathrm{w} - R_\mathrm{c}}{\overline{C}_\mathrm{w} - \overline{C}_\mathrm{c}} + Q \tag{1}$$

$$Q = u \cdot (R_\mathrm{w} - R_\mathrm{c})^2 \cdot \frac{(C_\mathrm{s} - \overline{C}_\mathrm{w}) \cdot (C_\mathrm{s} - \overline{C}_\mathrm{c})}{(\overline{C}_\mathrm{w} - \overline{C}_\mathrm{c})^2} \tag{2}$$

$R_s$ = Earth scene radiance
$R_w$ = warm calibration target radiance
$R_c$ = cold space radiance

$C_s$ = Earth scene counts

$\overline{C}_{\mathrm{w}}$ = warm target calibration measurement counts, averaged over four values

$\overline{C}_{\mathrm{c}}$ = cold space calibration measurement counts, averaged over four values

$Q$ = non-linear term

$u$ = non-linearity coefficient

In the following we discuss the uncertainties belonging to each term in the measurement equation and decide which ones could have caused the bias trends on the basis of the complete picture of the behavior of the instrument in flight. To simplify matters we assume that a difference of flux density expressed in K is proportional to the corresponding difference in W $\mathrm{cm}^{-2}$ $\mathrm{s}^{-1}$, i. e. the Rayleigh-Jeans approximation is applicable (see Sect. 2.3).

### 2.5.1 Non-linearity

The non-linearity correction coefficient is zero for all sounding channels of all AMSU-B flight models at all reference temperatures in the file of AMSU-B calibration parameters (`amsub_clparams.dat`, version 25) used by AAPP. In order to investigate whether a non-linearity developed during the mission we consider how the corresponding bias would change as a function of scene temperature, bearing in mind that $Q \propto (C_{\mathrm{s}} - \overline{C}_{\mathrm{w}}) \cdot (C_{\mathrm{s}} - \overline{C}_{\mathrm{c}})$. John et al. (2013a) find for Channel 20 - they call it Channel 5 - of AMSU-B on NOAA-16 a bias of about 3 K in the year 2008 relative to AMSU-B on NOAA-15, which is mainly due to an anomalous decreasing trend of unknown origin for N16. This bias is independent of the natural target chosen for the Earth scene, Antarctica or tropical oceans. Similar phenomena with AMSU-A were corrected by postulating a modified, time dependent $u$ (Zou and Wang , 2011). The values in Table 2, however, demonstrate that the bias should be ten times larger in observations of polar regions or the Moon than when derived from data collected over warm bodies of water, if it was due to non-linearity with AMSU-B as well. The reason is that the effect of the non-linearity on the calculated radiance becomes very small for scene temperatures close to those of the blackbody or the Cosmic Microwave Background. The brightness temperature of the atmosphere in Channel 20 is of course subject to variations, but even when we allow an uncertainty of a factor two in its difference to the temperature of the blackbody, the spread of values of $Q$ for the different scenes in Table 2 is incompatible with the observation that the biases depend very little on radiance. Non-linearity can therefore be ruled out as an explanation for the inter-channel trends.

### 2.5.2 Cold space temperature bias correction

The cold space temperature bias correction $\delta T_{c,ch}$ is for a given DSV the same for all sounding channels of AMSU-B on NOAA-16 in the file of calibration parameters (version 25) used by AAPP. It varies between 1.09 and 1.26 K Atkinson (2000b). In order to investigate whether the cold space temperature bias changed during the mission we consider how its impact varies with scene temperature, bearing in mind that in first approximation, i. e. neglecting the non-linearity term, $\delta T_{c,ch} \propto \frac{C_\mathrm{s} - \overline{C}_\mathrm{w}}{\overline{C}_\mathrm{w} - \overline{C}_\mathrm{c}}$. We make use of the same reasoning as in Sect. 2.5.1 by constructing a contradiction between expected and observed variation of the bias with scene brightness.

The values in Table 3 demonstrate that the bias should be 39 times larger in observations of the Moon than when derived from data collected over warm bodies of water. The reason is that the effect of the cold space temperature bias on the calculated radiance is largest for scene temperatures close to those of the Cosmic Microwave Background. Even when the bias in Channel 20 were only 1 K, a lower limit in view of the variations reported by John et al. (2013a), it would amount to an error of $\approx$ 39 K in the combined signal from Moon and CMB in the DSV. The actual error is at least an order of magnitude smaller (Burgdorf et al. , 2016), hence cold space temperature bias can be ruled out as an explanation for the inter-channel trends as well.

### 2.5.3 Warm target bias correction

The warm target bias correction $\delta T_{bb,ch}$ is zero for all sounding channels of all AMSU-B flight models at all reference temperatures in the file of AMSU-B calibration parameters (version 25) used by AAPP, except for channel 20 on FM3, where it is -0.16 K. Here the situation is just the opposite of the previous case inasmuch as the warm target bias affects the measurements less for lower scene temperatures. This is intuitively clear and follows from the fact that the second term of the sum on the right side of the measurement equation is negative for $C_\mathrm{s} \leq \overline{C}_\mathrm{w}$. The Moon intrusions do therefore not help to characterize effects originating in the blackbody. A warm target bias correction for channel 20 about ten times as large as the biggest value used by AAPP for any flight model would be needed. On top of that the correction for the other sounding channels would have to have opposite sign or be zero. While this possibility cannot be ruled out completely, it seems highly unlikely, especially given the fact that the Platinum Resistance Thermometers (PRTs) on the blackbody of the instrument in question gave no hint at dramatic alterations to the temperature pattern of the blackbody, see Fig. 2 and for a discussion of temperature drifts Hans et al. (2017).

### 2.5.4 Shift of channel center frequencies

Having discussed the main sources of error in the flux calibration we turn our attention to drifts of channel frequencies as a possible explanation of the bias that channel 20 exhibits when observing Earth scenes. An accurate value of $B(\nu + \delta\nu)$, i. e. the impact of a change in frequency on the measured flux, is difficult to calculate for channels 18 and 19, because the exact shape of the water vapor absorption line depends on the state of the atmosphere. It is possible, however, to give at least an estimate of the shift in frequency required to change the measured radiance by 0.4%, i. e. causing an error of about 1 K, for channel 20, because this one probes the well-characterized wings of the line profile (Bobryshev et al. , 2017). It amounts to 3.5 GHz. This value is 50 times larger than the specification for frequency stability (Atkinson , 2001). As all sounding channels use the same local oscillator (Saunders , 1995a), the same frequency shift would apply to channel 18 with ten times the effect on radiance. Such an enormous bias, however, is not observed.

### 2.5.5 Radio-frequency interference on NOAA-16

As we found no fault with the calibration of AMSU-B on NOAA-16, we searched for instrumental effects that could alter the counts used as input of the calibration process. Malfunction of the processing electronics can be ruled out, because the data from all channels are clocked into the same AMSU instrument processor. There is, however, another phenomenon with the potential to strongly affect the counts, namely radio-frequency interference (RFI). The bias it causes can be positive or negative and depends on channel, scan angle, and the transmitter in use. It was demonstrated in ground tests that AMSU-B on NOAA-16 was susceptible in all channels to radiation of the spacecraft transmitters (Ricketts and Atkinson , 1999). Modifications of the instrument, e. g. wrapping cables with electrically conductive aluminum tape, were carried out as a consequence of the problems encountered with AMSU-B on NOAA-15 and reduced this susceptibility by 1-2 orders of magnitude. From the NOAA-16 post launch orbital verification tests it was estimated that the remaining Earth-view biases, though difficult to quantify, are within $\pm$ 0.5 K when the transmitter is active (Atkinson , 2000a). During the lifetime of the satellite, however, the gain of the sounding channels decreased tremendously (see Table 1 and Hans et al. (2017)). A reduced gain produces a reduced signal, which means that interference becomes relatively more important, as described by John et al. (2013b). The overall reduction of signal during the mission lifetime due to gain degradation - a factor six for channel 19 between 2001 and 2010 - is of the same magnitude as the pre-launch reduction of interference, which came from about 6 K down to a little less than 1 K. Channel 19 is the channel that was most affected by RFI during tests on ground (Ricketts and Atkinson , 1999). We therefore conjecture that individual interference events caused a bigger and bigger bias over the years, but at the same time the noise equivalent difference in temperature (NE$\Delta$T) increased, making them still difficult to detect. We know from the experience with NOAA-15 that interference effects can be very different for Earth and space views, hence RFI could be absent in the observations of the Moon while still affecting $C_s$.

## 3 Conclusions

We have demonstrated that intrusions of the Moon in the DSV can be used to obtain otherwise inaccessible information about the characteristics of microwave sounders in flight. This is because the Moon provides a third flux reference, in addition to the CMB and the OBCT, with a spectrum that closely resembles a blackbody. This property makes it particularly suited for checks of the uniformity of sounding channels, where vicarious calibration is not an option. Another characteristic of the

Moon is that it fills only a fraction of the beams of past and present microwave sounders and therefore provides a flux level much lower than Earth scene and OBCT (see Fig. 3). As a consequence the Moon becomes a unique diagnostic tool for checking the cold space temperature bias correction and, in case of insufficient SNOs, non-linearity. Such characterisation of instrumental effects is essential for calculating uncertainties and harmonization coefficients of fundamental climate data records, as undertaken for example by the FIDUCEO project (FIDelity and Uncertainty of Climate data records from Earth Observations[3]).

In case of AMSU-B on NOAA-16 we found that the Moon signal from channel 20 agrees within 0.6% with the average signal of channels 18 and 19. It follows that

- The beam solid angle of channel 20 is within 0.3% the same as the average beam solid angle of channels 18 and 19, else they could not have given the same value for a source much smaller than OBCT and DSV.
- Any frequency shift of channel 20 must be smaller than $0.003 \cdot 183$ Ghz $\approx$ 500 MHz, else channel 20 would not agree with the other sounding channels.
- We attribute the bias in the sounding channels of AMSU-B on NOAA-16 to a simple and well-known effect, namely radio frequency interference, by eliminating all other possible causes. Although this finding needs confirmation by a careful investigation of the interference in flight, we recommend to exclude periods of active transmitters when calculating inter-calibration coefficients (Ferraro , 2015).
- One type of bias identified by Zou and Wang (2011) with AMSU-A, namely inaccurate calibration non-linearity, was ruled out in our investigation of AMSU-B. This finding provides evidence that the approach taken in the FIDUCEO project of harmonizing AMSU-B and MHS with the help of simultaneous nadir overpasses is sound, because the calculation of time-dependent nonlinear coefficients in flight, which would render that method impractical, is unnecessary.

Our characterization of sounding channels in flight demonstrates the potential of using intrusions of the Moon in the DSV as diagnostic tool for AMSU-B. Even higher accuracy is possible with MHS because of its lower NE$\Delta$T. In order to include also the window channels in the kind of analysis we presented, the differences of the brightness temperature of the Moon between the different radio wavebands must be known. A model describing them with the required accuracy is not available and remains therefore a worthwhile task for the future.

---

[3] `www.fiduceo.eu`

We conclude with a description of the potential of the Moon for in-orbit verification of future microwave imagers like MWI (MicroWave Imager). Because of its smaller beam, the method we described in this paper cannot be applied the same way, since the light curve will no longer have the shape of a Gaussian. This is because the finite size of the Moon and the asymmetric temperature distribution of its surface will cause deviations from the case of disk-integrated measurements. A specially defined scan profile - in the ideal case a two-dimensional raster map with a step size of 0.1° as proposed by Bonsignori (2017) - will then be advantageous. It will enable measurements of the Moon's flux with much better signal-to-noise ratio, because it will fill the whole beam, and it will provide several additional reference flux levels, because one can point at regions of the Moon with quite different temperatures. This way the non-linearity, to give just one example, can be characterised over a large flux range.

Author contributions I. Hans investigated the gain and noise changes, M. Prange investigated the stability of the OBCT and calculated, together with T. Lang, the values in Table 1. S. Buehler contributed to the text and helped with the interpretation and presentation of the results. M. Burgdorf prepared the manuscript with contributions from all co-authors.

**Data Sets:** The level 1b data from AMSU-B presented in this manuscript are available from NOAA CLASS (Comprehensive Large Array-data Stewardship System).

*Acknowledgements.* These characterisations are part of the effort to quantify the uncertainty budget for microwave sounders undertaken within the H2020 project, Fidelity and Uncertainty in Climate-data records from Earth Observation (FIDUCEO). FIDUCEO has received funding from the European Union's Horizon 2020 Programme for Research and Innovation, under Grant Agreement no. 638822. Stefan A. Buehler was partially supported by the Cluster of Excellence CliSAP (EXC177), Universität Hamburg, funded through the DFG, by the German Federal Ministry of Education and Research within the framework programme „Research for Sustainable Development (FONA)", under project HD(CP)2 (contracts O1LK1502B and O1LK1505D), and by the DFG HALO research program (contract BU2253/3-1). We are indepted to Christopher Merchant who noted several errors and inaccuracies in the draft version of the manuscript and to Oliver Lemke for contributing Fig. 1.

**Competing Interests:** The authors declare that they have no conflict of interest.

## References

Atkinson, N. C.: AMSU-B EM Thermal Vacuum Test Report, EM, Met Office, Farnborough, 18 pp., 2000.

Atkinson, N. C.: Performance of AMSU-B Flight Model 2 (FM2) during NOAA-L Post Launch Orbital Verification Tests, AMB112, Met Office, Farnborough, 24 pp., 2000.

Atkinson, N. C.: Calibration, Monitoring and Validation of AMSU-B, ADV SPACE RES, 28, 117-126, 2001.

Bobryshev, O., Brath, M., John, V., Buehler, S. A.: Is there really a closure gap between 183.31 GHz satellite passive microwave and in-situ radiosonde water vapor measurements?, accepted for publication in GEOPHYS RES LETT.

Bonsignori, R.: In-Orbit Verification of MHS Spectral Channels Co-registration Using the Moon, submitted to P SOC PHOTO-OPT INS. radiometers for MetOp Second Generation, Proc. of the 2012 CNIT Tyrrhenian Workshop, 2012.

Burgdorf, M. J., Buehler, S. A., Lang, T., Michel, S., Hans, I.: The Moon as a photometric calibration standard for microwave sensors, ATMOS MEAS TECH, 9, 3467-3475, 2016.

Burgdorf, M., Lang, T., Michel, S., Buehler, S. A., Hans, I.: The Moon as a diagnostic tool for microwave sensors, GSICS QUARTERLY, 10(2), 4-5, 2016.

Coates, R. J.: LUNAR BRIGHTNESS VARIATIONS WITH PHASE AT 4.3-MM WAVE LENGTH, ASTROPHYS J, 133, 723-725, 1961.

MHS Level 1 Product Generation Specification, https://www.eumetsat.int/website/home/Data/TechnicalDocuments/index.html, 17 September 2013.

Ferraro, R.: The Development of Advanced Microwave Sounding Unit-B (AMSU-B) and Microwave Humidity Sounder (MHS) Fundamental Climate Data Records (FCDR) for Hydrological Applications, DSR, CDR Program, 37 pp., 2015.

Hanlon, H. and Ingram, W.: Fundamental Climate Data Record of Microwave Brightness Temperatures, CM-150, EUMETSAT Satellite Application Facility on Climate Monitoring, 2015.

Hans, I., Burgdorf, M., John, V. O., Mittaz, J., Buehler, S. A.: Noise performance of microwave humidity sounders over their life time, submitted to ATMOS MEAS TECH.

John, V. O., Holl, G., Buehler, S. A., Candy, B., Saunders, R. W., Parker, D. E.: Understanding intersatellite biases of microwave humidity sounders using global simultaneous nadir overpasses, J GEOPHYS RES-ATMOS, 117, D02305, 2012.

John, V. O., Allan, R. P., Bell, W., Buehler, S. A., Kottayil, A.: Assessment of intercalibration methods for satellite microwave humidity sounders, J GEOPHYS RES-ATMOS, 118, 4906-4918, 2013.

John, V. O., Holl, G., Atkinson, N., Buehler, S. A.: Monitoring scan asymmetry of microwave humidity sounding channels using simultaneous all angle collocations, J GEOPHYS RES-ATMOS, 118, 1-10, 2013.

Labrot, T., Lavanant, L., Whyte, K., Atkinson, N., Brunel, P.: AAPP Documentation Scientific Description, NWPSAF-MF-UD-001, Satellite Application Facility for Numerical Weather Prediction, 107 pp., 2011.

Keihm, S. J.: A Lunar Calibration Model for the COBE DMR Experiment, Interoffice Memorandum, Jet Propulsion Laboratory, Pasadena, 1983.

McLellan, S.: Performance of AMSU-B Proto-Flight Model (PFM) during NOAA-K Post Launch Orbital Verification Tests, AMB106, Meteorological Office, Farnborough, 11 pp., 1998.

Mangum, J. G.: Main-Beam Efficiency Measurements of the Caltech Submillimeter Observatory, PUBL ASTRON SOC PAC, 105, 117-122, 1993.

Moradi, I., Meng, H., Ferraro, R. R., Bilanow, S.: Geolocation and Scan Asymmetry Correction for NOAA POES Passive Microwave Instruments, IEEE T GEOSCI REMOTE, 51, 3625-3637, 2013.

Ricketts, M. V. and Atkinson, N. C.: Pre-shipment EMC Susceptibility Tests for AMSU-B FM2 (August 1999), 6 pp.

Saunders, R. W.: AMSU-B Calibration, Meteorological Office, Farnborough, 38 pp., 1994.

Saunders, R. W.: Results of AMSU-B Radiometric Characterisation Tests, Meteorological Office, Farnborough, 27 pp., 1995.

Saunders, R. W., Hewison, T. J., Stringer, S. J., Atkinson, N. C.: The Radiometric Characterization of AMSU-B, IEEE T MICROW THEORY, 43, 760-771, 1995.

Weng, F. and Yang, H.: Validation of ATMS Calibration Accuracy Using Suomi NPP Pitch Maneuver Observations, REMOTE SENS-BASEL, 8, 332-346, 2016.

Yang, H. and Weng, F.: Corrections for On-Orbit ATMS Lunar Contamination, IEEE T GEOSCI REMOTE, 54, 1918-1924, 2016.

Zou, C.-Z. and Wang, W.: Intersatellite calibration of AMSU-A observations for weather and climate applications, J GEOPHYS RES, 116, D23113, 2011.

**Table 1.** Results from Gaussian fits to the light curves of Moon intrusions in DSVs of AMSU-B on NOAA-16. Columns 1 and 2: date and time of occurence of smallest lunar angle, columns 3-5: gain in counts/K, column 6: number of DSV pixel closest to the Moon, column 7: minimum lunar angle as calculated with AAPP, column 8: minimum lunar angle as calculated from maximum signal in each DSV, column 9: ratio of brightness temperatures in channels 18/19 (averaged) and channel 20.

| Date | Time | Gain 18 | Gain 19 | Gain 20 | DSV | Pos. (AAPP) | Pos. (Gauss) | $T_{18/19}/T_{20}$ |
|---|---|---|---|---|---|---|---|---|
| 1/4, 2001 | 16:14 | 21.05 ± 0.07 | 16.71 ± 0.05 | 10.87 ± 0.04 | 4 | −0.02° | | 0.9944 |
| 1/6, 2001 | 2:58 | 21.03 ± 0.09 | 16.71 ± 0.06 | 10.87 ± 0.05 | 2 | −0.09° | +0.12° | 0.9523 |
| 1/6, 2001 | 4:40 | 21.03 ± 0.07 | 16.70 ± 0.06 | 10.85 ± 0.05 | 1 | +0.11° | | 0.9947 |
| 2/3, 2001 | 9:34 | 21.11 ± 0.09 | 16.83 ± 0.07 | 10.91 ± 0.05 | 1 | +0.02° | | 0.9751 |
| 2/3, 2001 | 23:23 | 21.10 ± 0.10 | 16.83 ± 0.06 | 10.90 ± 0.04 | 1 | +0.02° | | 1.0073 |
| 1/1, 2004 | 14:02 | 17.34 ± 0.07 | 13.83 ± 0.05 | 9.34 ± 0.04 | 2 | −0.12° | −0.04° | 0.9982 |
| 1/3, 2004 | 2:13 | 17.29 ± 0.08 | 13.81 ± 0.06 | 9.31 ± 0.04 | 2 | | −0.03° | 0.9897 |
| 4/29, 2004 | 11:41 | 16.54 ± 0.07 | 13.29 ± 0.05 | 8.98 ± 0.04 | 2 | −0.22° | −0.13° | 1.0127 |
| 5/29, 2004 | 7:14 | 16.47 ± 0.07 | 13.23 ± 0.06 | 8.92 ± 0.04 | 2 | −0.21° | −0.10° | 0.9929 |
| 5/29, 2004 | 22:19 | 16.49 ± 0.07 | 13.26 ± 0.05 | 8.95 ± 0.03 | 2 | −0.25° | −0.11° | 0.9520 |
| 11/23, 2004 | 9:36 | 15.54 ± 0.06 | 12.58 ± 0.04 | 8.84 ± 0.03 | 2 | −0.22° | −0.12° | 1.0606 |
| 12/21, 2004 | 6:46 | 15.25 ± 0.06 | 12.39 ± 0.04 | 8.35 ± 0.04 | 3 | −0.07° | −0.01° | 0.9914 |
| 4/8, 2006 | 19:58 | 10.86 ± 0.06 | 9.33 ± 0.04 | 6.08 ± 0.04 | 4 | −0.36° | | 0.9529 |
| 5/8, 2006 | 17:07 | 10.47 ± 0.05 | 9.01 ± 0.05 | 5.84 ± 0.04 | 2 | +0.08° | +0.15° | 1.0024 |
| 11/2, 2006 | 12:36 | 8.37 ± 0.06 | 7.47 ± 0.04 | 4.71 ± 0.04 | 1 | +0.02° | | 1.0457 |
| 11/2, 2006 | 14:17 | 8.34 ± 0.05 | 7.46 ± 0.05 | 4.69 ± 0.05 | 2 | −0.04° | −0.12° | 0.9692 |
| 12/2, 2006 | 5:28 | 7.98 ± 0.08 | 7.19 ± 0.05 | 4.48 ± 0.04 | 4 | +0.03° | | 1.0643 |
| 12/2, 2006 | 14:07 | 7.96 ± 0.08 | 7.18 ± 0.05 | 4.47 ± 0.05 | 4 | +0.03° | | 0.9906 |
| 3/29, 2007 | 12:55 | 7.22 ± 0.06 | 6.61 ± 0.05 | 4.07 ± 0.04 | 2 | −0.12° | +0.06° | 0.9819 |
| 3/31, 2007 | 9:51 | 7.12 ± 0.05 | 6.54 ± 0.05 | 4.01 ± 0.04 | 2 | −0.03° | +0.03° | 1.0012 |
| 11/22, 2007 | 15:03 | 4.96 ± 0.05 | 4.80 ± 0.04 | 2.81 ± 0.03 | 2 | −0.11° | −0.20° | 1.0465 |
| 11/22, 2007 | 21:57 | 5.02 ± 0.05 | 4.85 ± 0.04 | 2.84 ± 0.03 | 3 | −0.06° | −0.03° | 1.0237 |
| 11/22, 2007 | 23:41 | 4.99 ± 0.06 | 4.83 ± 0.04 | 2.83 ± 0.04 | 3 | −0.08° | +0.02° | 0.9810 |
| 11/23, 2007 | 1:25 | 4.95 ± 0.06 | 4.79 ± 0.05 | 2.81 ± 0.04 | 3 | −0.15° | −0.07° | 0.9812 |
| 11/23, 2007 | 6:35 | 4.90 ± 0.08 | 4.75 ± 0.05 | 2.78 ± 0.04 | 2 | 0.00° | +0.05° | 1.0358 |
| 2/19, 2008 | 6:09 | 3.68 ± 0.08 | 3.73 ± 0.07 | 2.09 ± 0.05 | 1 | −0.03° | | 1.0291 |
| 10/13, 2008 | 9:23 | 4.11 ± 0.07 | 4.53 ± 0.04 | 2.45 ± 0.03 | 3 | −0.22° | −0.10° | 0.9928 |

**Table 2.** The relative value of the non-linearity term $Q$ in the measurement equation for different scenes. The counts are from channel 20 in the orbit of the last Moon intrusion listed in Table 1, i. e. measured in October 2008. $Q_0$ is the non-linearity correction for observations over tropical ocean.

| Scene | Counts | $Q$ / $Q_0$ |
|---|---|---|
| Tropical Ocean | 15,200 | 1 |
| Polar Regions | 15,100 | 11 |
| Moon | 14,635 | 9 |
| Black Body | 15,215 | 0 |
| Deep Space | 14,540 | 0 |

**Table 3.** Relative value of the cold space bias correction $\delta T$ in the measurement equation for different scenes - the counts are from channel 20 in the orbit of the last Moon intrusion listed in Table 2, i. e. measured in October 2008. $\delta T$ is the change in the calculated scene temperature due to the cold space temperature bias correction, where the subscript 0 indicates the value for observations over tropical ocean.

| Scene | Counts | $\frac{\delta T}{\delta T_0}$ |
|---|---|---|
| Tropical Ocean | 15,200 | 1 |
| Polar Regions | 15,100 | 8 |
| Moon | 14,635 | 39 |
| Black Body | 15,215 | 0 |
| Deep Space | 14,540 | 45 |

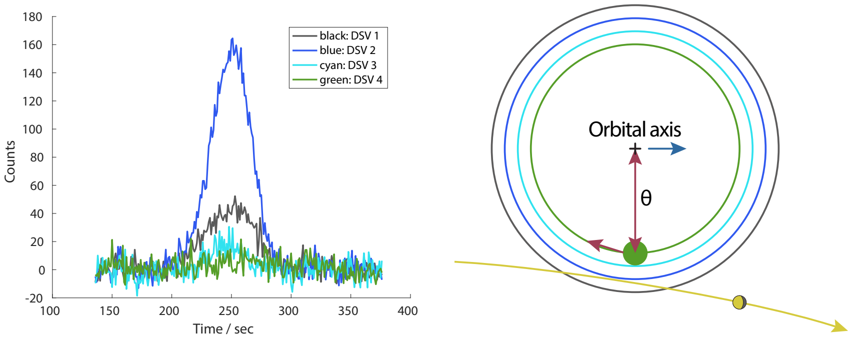

**Figure 1.** Left: Light curves of the Moon obtained from the four AMSU-B deep space views (pixels) on 11/2, 2006. Right: Observing geometry projected to the sky: The axis of the orbit of the satellite is marked with a plus sign. $\theta = 9.5^\circ$ is its angular distance from DSV 4, shown as a filled, green circle. The pointing direction of the instrument describes a great circle in the sky during one scan, which covers all four deep space views and then continues along the large, red arrow. From one scan to the next, all DSVs move by a small amount along the large circles in the orientation of the small red arrow. The yellow arrow gives an example of the trajectory of the Moon. DSV 2 came closest and gave therefore the highest signal in its light curve. DSV 4 was too far away from the Moon to be affected by its presence. From the ratio of the maximum signals in DSV 1 and DSV 3 one can caluclate how far the Moon is away from DSV 2. This distance is zero if and only if the counts from DSV 1 and DSV 3 are the same. The completion of the circles that each DSV desribes in the sky takes 100 min, the duration of the orbit of the satellite. This is fast compared to the movement of the Moon (synodic month 29.5 days) and the movement of the orbital axis of the satellite with a period of one year (blue arrow).

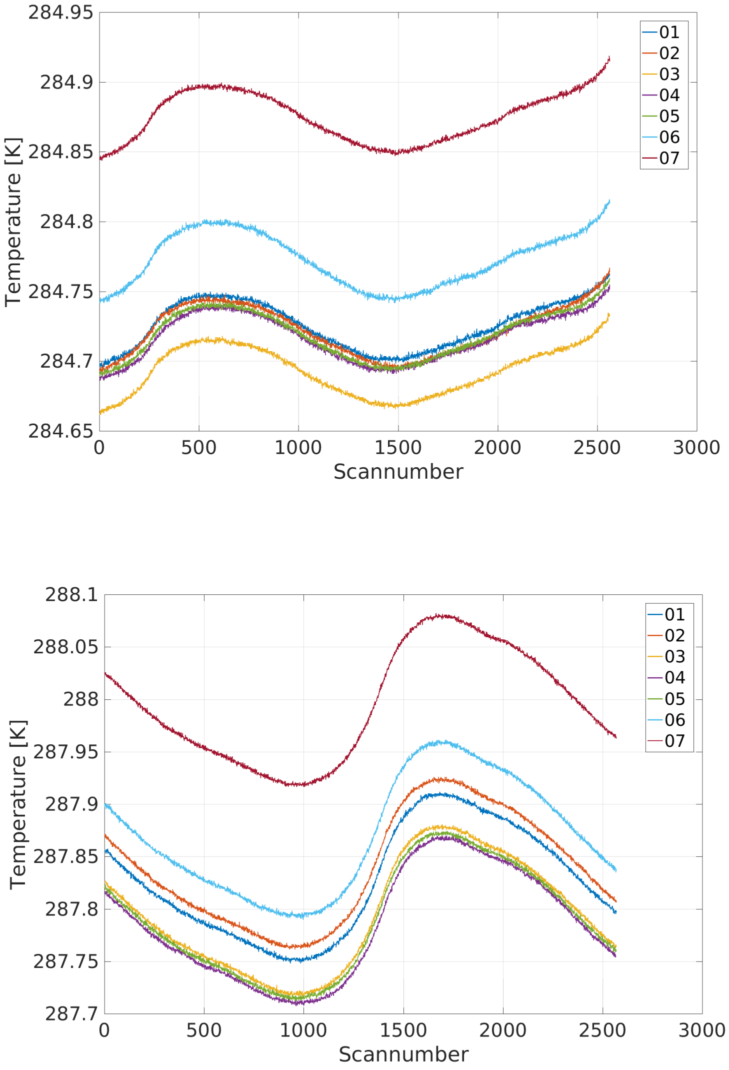

**Figure 2.** Temperature measured by seven PRTs of the blackbody of AMSU-B on board NOAA-16 during two orbits ten years apart: 2/12, 2001 (top) and 7/30, 2011 (bottom)

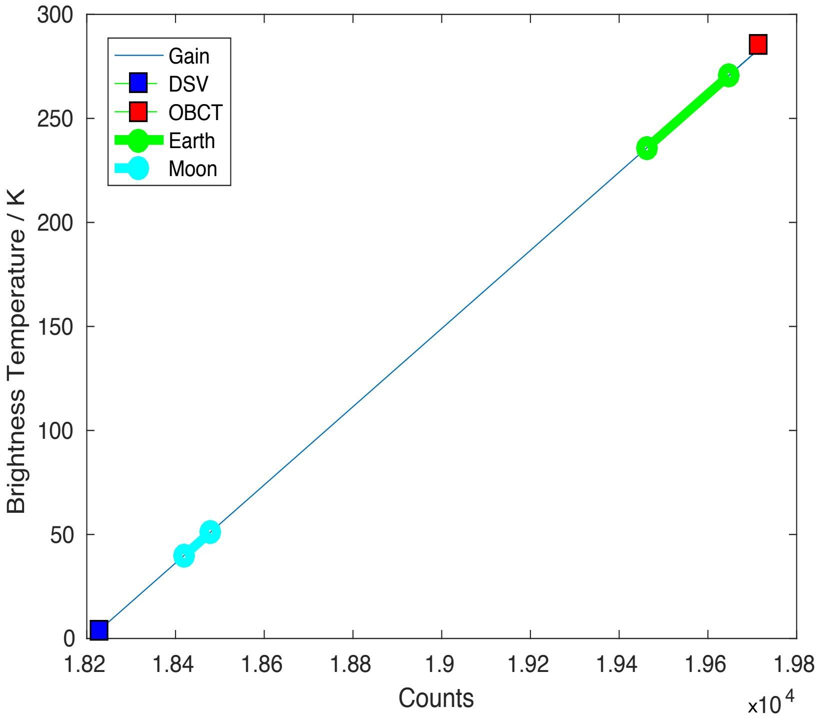

**Figure 3.** Schematic representation of the signal range in counts and brightness temperature covered by deep space, Moon scenes, Earth scenes, and internal calibration target for channel 20 of AMSU-B on NOAA-16 in 2006. A gain of 5 counts/K was assumed. The Moon gives a much lower signal than the Earth, because it fills only a fraction of the beam.